Effect of Carbon Nanotube Addition on Structure and Properties for Extrudates of High-Density Polyethylene

Riho Nishikawa and Masayuki Yamaguchi*

School of Materials Science, Japan Advanced Institute of Science and Technology,

1-1 Asahidai, Nomi, Ishikawa 923-1292, JAPAN

*Corresponding author

E-mail address: m_yama@jaist.ac.jp (Masayuki Yamaguchi)

Phone: +81-761-51-1621

Fax: +81-761-51-1149

ABSTRACT

We investigated the structure and properties of strands of high-density polyethylene (HDPE), containing multi-walled carbon nanotubes (MWCNTs) extruded from a capillary rheometer. Surprisingly, we found that the MWCNTs enhanced the chain orientation of HDPE, and that in the absence of MWCNTs, orientation relaxation occurred in the HDPE immediately after passing through the die. Conventional differential scanning calorimetry measurements indicated that MWCNT acts as a nucleating agent and raises the crystallization temperature 2 - 4 °C under quiescent condition. In the flow field, oriented MWCNTs behave like polymeric chain extended crystals “shish”, and greatly accelerate the flow-induced crystallization of the HDPE “kebab”. Consequently, the modulus was significantly increased in the flow direction. These findings demonstrate that the addition of MWCNTs is an effective method of enhancing the rigidity of HDPE.

1. Introduction

Recent developments in industrial-scale carbon nanotube (CNT) production have greatly accelerated scientific research. CNTs are often used as fillers for thermoplastic and thermosetting resins to effectively enhance their Young's modulus and strength.[1–3] As well as increasing the modulus by providing reinforcement, CNTs act as nucleating agents in some crystalline polymers, thereby increasing crystallinity and further enhancing the modulus. Moreover, rapid crystallization by the addition of CNTs often leads to enhanced molecular orientation, which is also responsible for the marked rigidity.[4–6]

The "shish-kebab" is one of the well-known structures generated in actual processing operations besides oriented spherulites.[7,8] Because it is composed of an extended crystalline part, i.e., shish, and lamellae developed from the shish, i.e., kebab, the structure provides a high degree of molecular orientation. With regard to polyethylene (PE), two types of lamellar growing are known: the *a*-structure (Keller–Machin type I) and the *c*-structure (Keller–Machin type II).[9] In both structures, the long axis of the lamellae (the *b*-axis) orients perpendicular to the flow direction. In the *a*-structure, the lamellae twist as they grow, and the flat faces of the lamellae (in the *a*-axis) become strongly oriented to the flow direction; i.e., the *a*-axis is preferentially oriented to the flow direction rather than the *c*-axis. Therefore, it is not a regular twisting like lamellae in spherulites. In contrast, in the *c*-structure, the chain-axis (the *c*-axis) of the lamellae orients to the flow direction. Both structures are easily identified by their two-dimensional wide-angle X-ray diffraction patterns. In general, the *a*-structure appears in PE products obtained under relatively low strain, whereas the *c*-structure forms under conditions of high strain and prompt crystallization. In both cases, the initial stage of structure development is the formation of shish, i.e., the crystallization of polymeric extended chains.[10] Therefore, the prompt formation of shish accelerates the whole crystallization rate. This can be achieved by adding a high-molecular-weight fraction with a Rouse relaxation time that is

longer than the inverse of the strain rate.[11–17] As well as high-molecular-weight components, fibrous nucleating agents also behave like "shish", greatly affecting the processability, structure, and properties of the polymer in the solid state.[18–21]

In the present study, we focused on the strong nucleating ability of multi-walled carbon nanotubes (MWCNTs) in high-density polyethylene (HDPE). We investigated the effect of MWCNTs on shish-kebab formation using a capillary rheometer. Although it has been known that CNTs show nucleating activity for PE, the crystallization under the flow field has not been reported so much.[22–24] Moreover, the details in the crystalline structure of PE grown on the MWCNT surface are still unknown.[25] Since the relaxation time of the MWCNT orientation is long compared with the characteristic time under the flow,[26] i.e., the inverse of the shear rate, MWCNTs can behave like shish at conventional processing operations. We found that MWCNTs enhance the chain orientation of HDPE to a surprising extent. Therefore, the addition of MWCNTs is an effective new method for enhancing the rigidity of HDPE.

2. Experimental Section

2.1 *Materials*

We used HDPE with a melt flow rate (MFR) of 40 g/10 min (HJ590N; Japan Polyethylene Corp., Japan) in the present study. The number- and weight-average molecular weights—characterized by size exclusion chromatography at 140 °C using 1,2,4-trichlorobenzene as an eluent—are M_n = 8.7 × 10^3 and M_w = 4.9 × 10^4 as a polyethylene standard; the density at 23 °C is 960 kg/m^3.

A composite comprising HDPE and 3 wt.% MWCNTs (NT-7; Hodogaya Chemical Co., Ltd., Japan), i.e., HDPE/MWCNT (3 wt.%), was kindly provided in pellet form by Hodogaya Chemical Co., Ltd. and employed as a master batch. The diameter of the MWCNTs ranged from 40 to 80 nm, their length was between 10 and 20 μm, and their density was 2300 kg/m^3;

further details are described elsewhere.[27] We reported that the MWCNTs employed are well dispersed in thermoplastics including HDPE without bundle structure by conventional melt-mixing.[27–30]

2.2 *Sample preparation*

The melt-mixing of HDPE/MWCNT (3 wt.%) and pure HDPE was performed using an internal batch mixer (Labo-Plastmill, Toyo Seiki Seisakusyo, Japan) at 160 °C. The blade rotation speed was 50 rpm and the duration of mixing was 5 min. The MWCNT contents were 0, 0.1, 0.3, and 1.0 wt.%. The samples were then compression-molded at 300 °C for 3 min to prepare flat films with 900 μm thickness for the rheology measurements. For the extrusion by a capillary rheometer, the films were cut into small pieces.

We carried out extrusion at 160 °C using a capillary rheometer (140 SAS-2002, Yasuda Seiki Seisakusho, Ltd., Japan) at apparent wall shear rates of 36.5 and 1000 s^{-1}. We used three types of circular dies with length (L)-to-diameter (D) ratios of 3/1, 20/1, and 40/1 (mm). The entrance angle of the dies was 180°. One strand was extruded downward from a die without stretching and cooled in the air atmosphere at 23 °C. The strands obtained had uniform diameter with smooth surface. After collecting the strands, we evaluated the crystallization temperature by differential scanning calorimetry measurements and the structure by two-dimensional wide- and small-angle X-ray measurements and the dynamic tensile modulus.

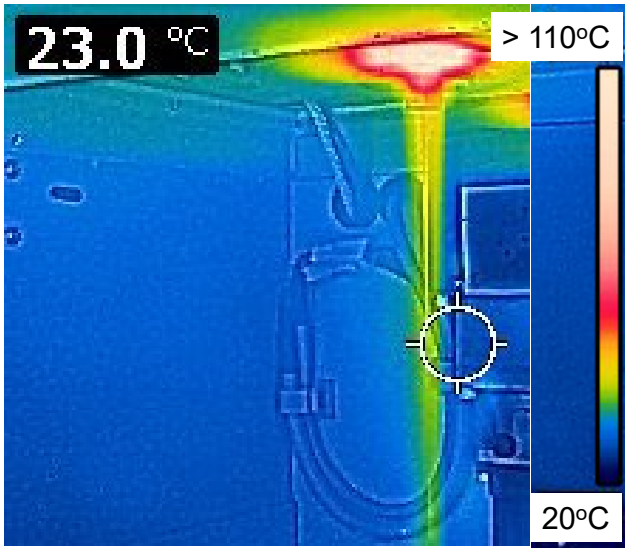

Fig. 1. Picture of thermal imaging camera

At the capillary extrusion, we evaluated the cooling rates of the strands using an infrared thermal imaging camera (FLIR C2, FLIR Systems, Inc., USA). The accuracy of the machine is ±2 °C and the measurement pixels are 4800. Fig. 1 shows the picture of the thermal imaging camera for the capillary rheometer and the extruded strand.

2.3 *Measurements*

The angular frequency dependence of the oscillatory shear moduli was measured using a rheometer (AR2000ex, TA Instruments, Inc., USA) at 160 °C under a nitrogen atmosphere. A cone-and-plate geometry (cone diameter was 25 mm and cone angle was 4 °) was employed for pure HDPE, while a parallel-plate geometry (25 mm in diameter) was for the composites. The angular frequency range was 0.01–628.3 rad/s.

The steady-state shear stress was measured by the capillary rheometer with a circular die of an L/D=20/1 at 160 °C. Neither Bagley and Rabinowitsch corrections were performed; i.e., the apparent values on the wall were collected.

The crystallization temperature was evaluated using the strands by a differential scanning calorimeter (DSC) (DSC8500, PerkinElmer Co., Ltd., USA) under a nitrogen atmosphere. After complete melting at 230 °C for 3 min, the sample was cooled to 50 °C at cooling rates of 10 and 100 °C/min. The amount of the sample was approximately 10 mg for the slow cooling (10 °C/min) and 1 mg for the fast one (100 °C/min).

Two-dimensional wide-angle X-ray diffraction (WAXD) and small-angle X-ray scattering (SAXS) patterns of the extruded strands were collected by an XRD machine (SmartLab, Rigaku Corp., Japan) with an imaging plate. A graphite-monochromatized Cu Kα radiation beam, operated at 45 kV and 200 mA, was inserted into the strands. The exposure was performed with 1 min a shot for WAXD and 30 min for SAXS.

The tensile storage modulus at 20 °C was evaluated by a dynamic mechanical analyzer (Rheogel-E4000, UBM Co. Ltd., Japan) using extruded strands at 10 Hz. The oscillatory strain was applied in the parallel direction of the strand extruded at 36.5 s^{-1}. The initial distance between the gages was 10 mm. The sinusoidal strain in the linear region, approximately 0.3%, was applied to the strand.

3. Results and discussion

3.1 *Characterization of the composites*

The rheological properties in the molten state were evaluated by a cone-and-plate rheometer for linear viscoelastic properties and a capillary rheometer for steady-state shear stress using compression-molded films. Fig. 2 shows the angular frequency dependence of the oscillatory shear moduli—i.e., the storage modulus G' and the loss modulus G''—for the samples containing various amounts of MWCNTs at 160 °C.

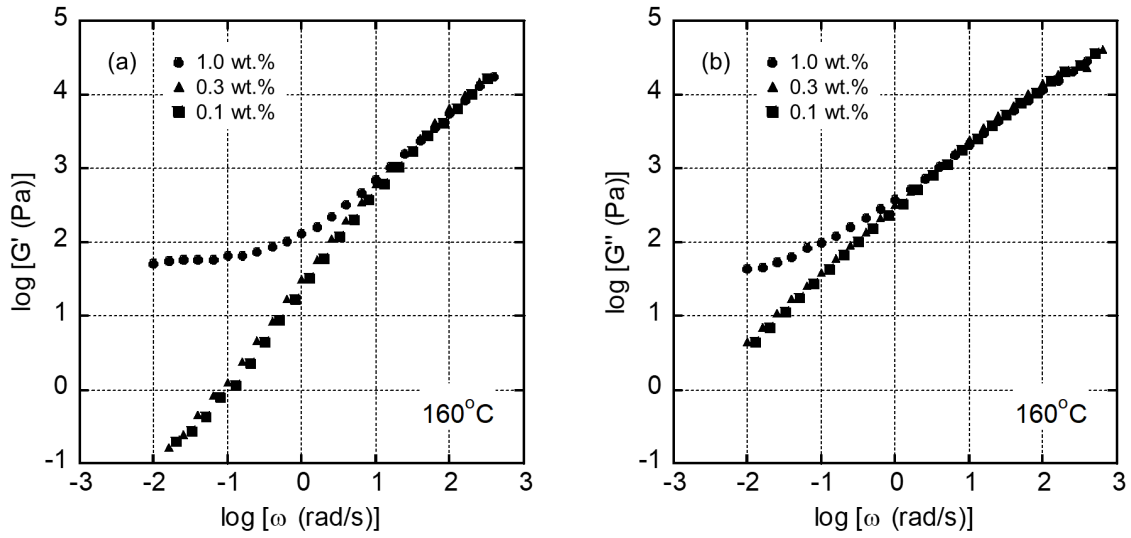

Fig. 2. Angular frequency dependency of (a) shear storage modulus G' and (b) loss modulus G'' at 160 °C for the samples containing various amounts of MWCNTs.

As the figure illustrates, both the G' and G'' of the samples containing 0.1 and 0.3 wt.% of MWCNTs decreased with decreasing frequency. The moduli were almost the same with those of the pure HDPE. This is the typical viscoelastic behavior of the rheological terminal region of a simple polymer melt. In other words, the small amounts of MWCNTs (≤ 0.3 wt.%) did not affect the linear viscoelastic properties in this experimental range. In contrast, the slopes of G' and G'' were small for the sample with 1.0 wt.% of MWCNTs, suggesting that a secondary plateau appeared owing to the network structure of the MWCNTs. This is a well-known rheological behavior for an MWCNT-dispersion system.[29,31–33]

Fig. 3 shows the flow curves evaluated using the capillary rheometer with a circular die of an L/D=20/1, i.e., the apparent shear stress on the wall σ_w plotted against the apparent shear rate on the wall $\dot{\gamma}_w$. The steady-state shear stress for the sample containing 1.0 wt.% of MWCNTs was almost the same with those for the others, although the oscillatory shear modulus was different. This is a typical flow curve for a suspension containing rigid rods.[34,35] Since the MWCNTs orient to the flow direction, the interparticle interaction is reduced.

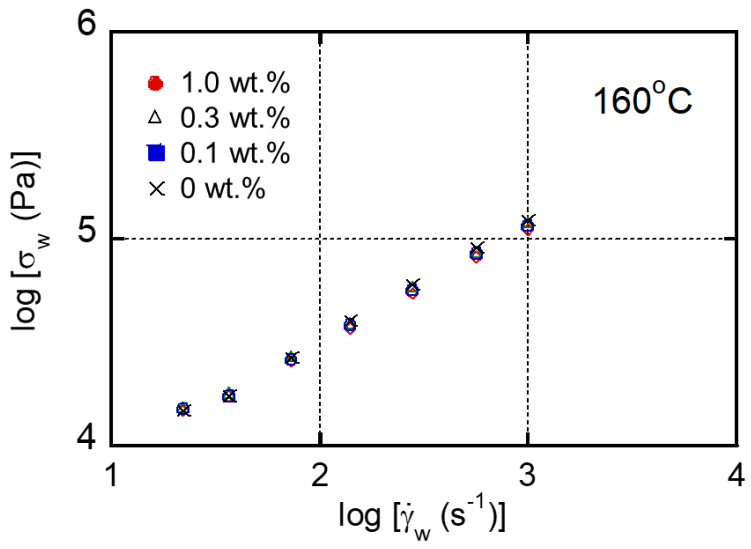

Fig. 3. Steady-state shear stress on the wall σ_w plotted against the apparent shear rate on the wall $\dot{\gamma}_w$ at capillary extrusion at 160 °C for the samples with various amounts of MWCNTs.

Fig. 4 shows the DSC cooling curves at two different rates using the extruded strands. Prior to cooling, the thermal history was erased at 230 °C for 3 min. The onset and peak temperatures of crystallization were summarized in Fig. 5. It was found that the MWCNTs increased the crystallization temperature; i.e., MWCNTs act as nucleating agents for HDPE. According to Li et al.,[36] the nucleating activity of CNTs for PE is attributed to the soft epitaxy, at which both epitaxy and geometry confinement accelerate the crystallization. Since the enhancement of the crystallization temperature was obvious even by a small amount (0.1 wt.%), the MWCNTs used in this study have the strong nucleating activity. Furthermore, the figure indicated that the gap between the onset and maximum crystallization temperatures is more prominent at the fast cooling rate, i.e., 100 °C/min, which was not strongly affected by the MWCNT addition at this experimental condition.

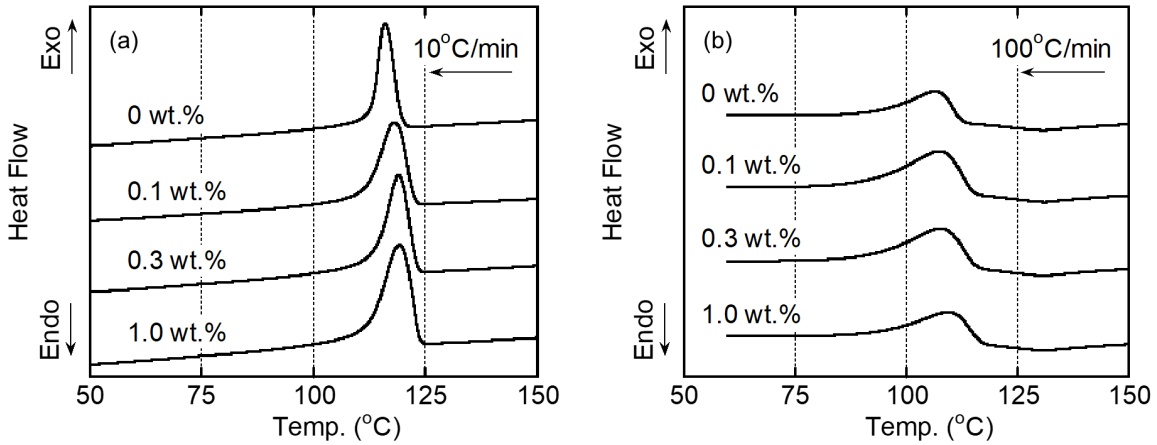

Fig. 4. Differential scanning calorimeter (DSC) curves at cooling rates of (a) 10 °C/min and (b) 100 °C/min.

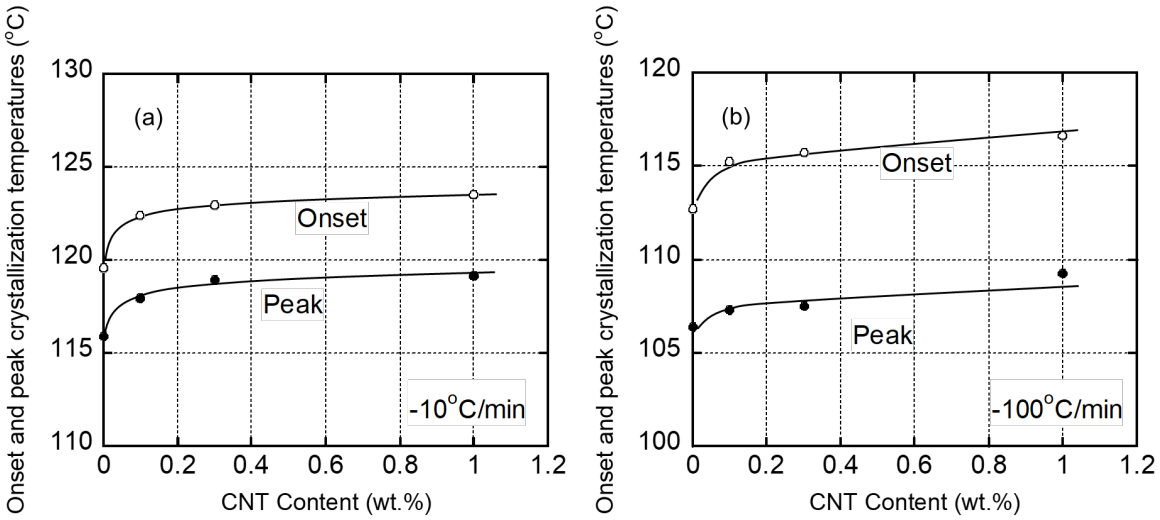

Fig. 5. Crystallization onset and peak temperatures as a function of the MWCNT content at cooling rates of (a) 10 °C/min and (b) 100 °C/min.

3.2 *Characterization of the extruded strands*

The samples were extruded by the capillary rheometer with a circular die (L/D=20/1). We estimated the cooling rates of the strands using the thermal imaging camera, and found them to be 3.8 °C/s (2.3 × 10^2 °C/min) at 36.5 s^{-1} and 70 °C/s (4.2 × 10^3 °C/min) at 1000 s^{-1}, which are typical values at capillary extrusion.[37–39]

Fig. 6 shows two-dimensional wide-angle X-ray diffraction (2D-WAXD) images of the strands extruded at 36.5 s^{-1} and 1000 s^{-1} as apparent shear rates on the wall. Because X-ray went through whole strands, the images obtained the information on not only surface but also core in the strands (the average shear rates are, therefore, 18.3 s^{-1} and 500 s^{-1}, respectively).

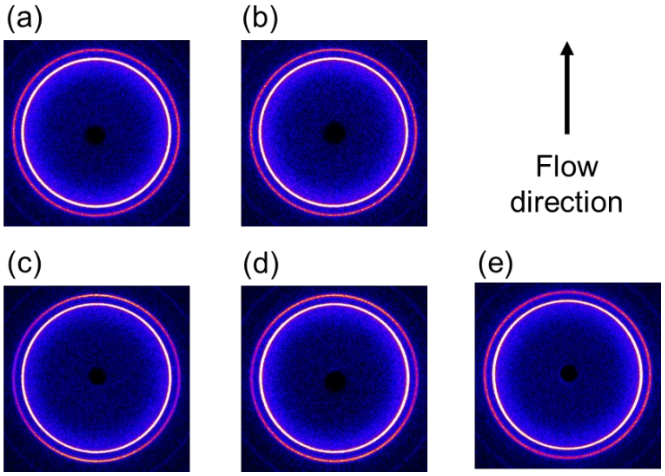

Fig. 6. Two-dimensional wide-angle X-ray diffraction (2D-WAXD) images of extruded strands: (a) HDPE at 36.5 s^{-1}, (b) HDPE at 1000 s^{-1}, (c) 0.1 wt.% of MWCNTs at 36.5 s^{-1}, (d) 0.3 wt.% of MWCNTs at 36.5 s^{-1}, and (e) 1.0 wt.% of MWCNTs at 36.5 s^{-1}. The shear rates are the values on the wall.

The integrated intensity data are plotted against 2θ in Fig. 7. There are two distinct peaks, which are ascribed to the (110) and (200) planes of HDPE (the numbers in brackets are the Miller indices), and which are easily discernable from the broad amorphous background. The degree of crystallization χ, denoted in the figure, was calculated from the following equation,

$$\chi = \frac{\sum_i I_{c_i}}{\sum_i I_{c_i} + I_a} \tag{1}$$

where I_c and I_a are the areas of crystalline and amorphous peaks. It was found that the MWCNT addition slightly increased the crystallinity. This is owing to the enhanced packing of crystalline region by the alignment of lamellar crystals, which will be shown later.

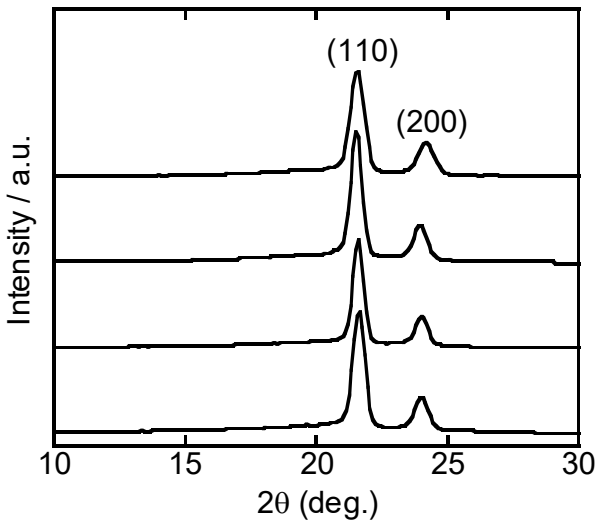

Fig. 7. Integrated intensity data plotted against 2θ for the strands extruded at 36.5 s^{-1}.

The type of lamellar growth—i.e., either *a*-structure (twisted lamellae) or *c*-structure (untwisted lamellae)—can be determined by the azimuthal distribution of the diffraction peaks. Fig. 8 shows the azimuthal distribution of the (110) and (200) planes. There was almost no orientation in the HDPE, even at 1000 s^{-1}. This suggests that the molecular orientation induced by the capillary die is relaxed prior to the crystallization. In contrast, the azimuthal distribution demonstrates that the MWCNT addition provides the chain orientation. The blends with 0.1 and 0.3 wt.% of MWCNTs had the strong intensity at 0 and 180 degrees (meridian) for the (200) plane. Correspondingly, each equatorial peak of the (110) plane was divided into two. The profiles suggested that they have *a*-structure (twisted lamellae) even at 36.5 s^{-1}. Moreover, the blend containing 1.0 wt.% of MWCNTs exhibited the strong intensity at 90 and 270 degrees (equator) for both the (110) and (200) planes, demonstrating that it has *c*-structure (untwisted lamellae). These results indicated that the MWCNT addition greatly increases the orientation

of PE chains. Prompt crystallization on the surface of the MWCNTs aligned to the flow direction prohibits the orientation relaxation of the PE chains, thereby ensuring a high degree of orientation.

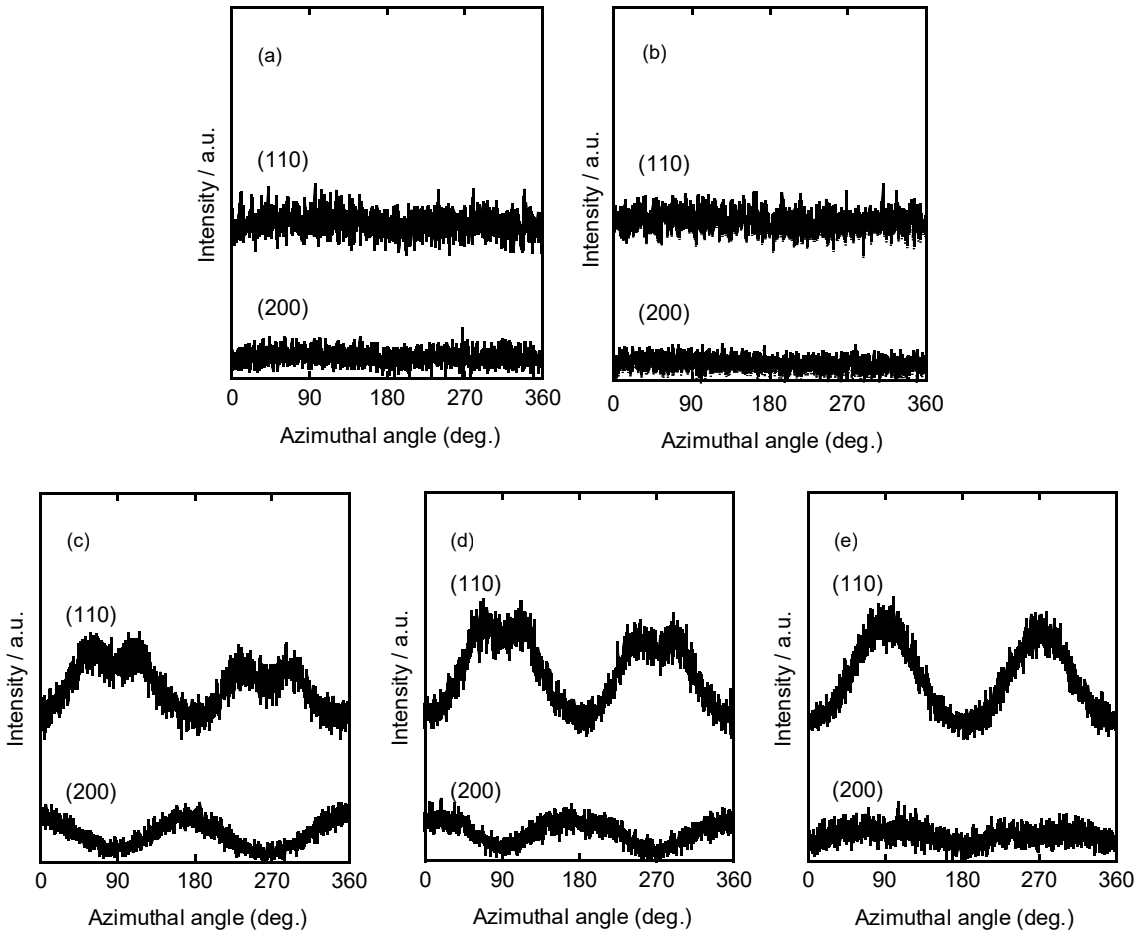

Fig. 8. Azimuthal distribution of (110) and (200) planes: (a) HDPE at 36.5 s^{-1}, (b) HDPE at 1000 s^{-1}, (c) 0.1 wt.% of MWCNTs at 36.5 s^{-1}, (d) 0.3 wt.% of MWCNTs at 36.5 s^{-1}, and (e) 1.0 wt.% of MWCNTs at 36.5 s^{-1}. The shear rates are the values on the wall.

Fig. 9 shows two-dimensional small-angle X-ray scattering (2D-SAXS) images. As shown in the figure, the strands containing MWCNTs exhibited the strong intensity in meridian, indicating the lamellae orient perpendicular to the flow direction. This corresponds with the

WAXD results. The long axis, derived from the intensity distribution in the vertical direction, was approximately 20 nm for all samples.

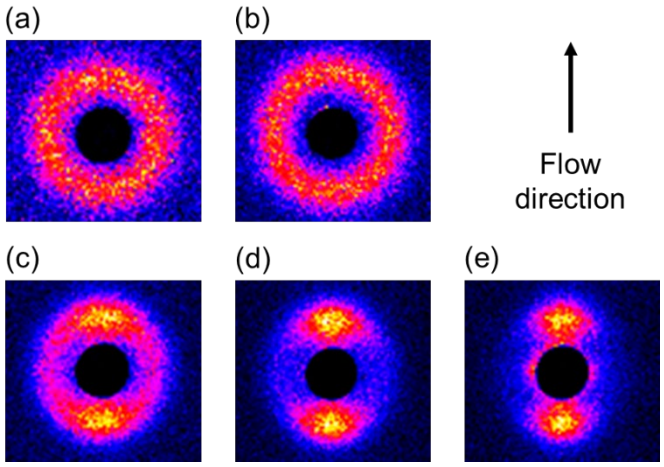

Fig. 9. Two-dimensional small-angle X-ray scattering (2D-SAXS) images of extruded strands: (a) HDPE at 36.5 s^{-1}, (b) HDPE at 1000 s^{-1}, (c) 0.1 wt.% of MWCNTs at 36.5 s^{-1}, (d) 0.3 wt.% of MWCNTs at 36.5 s^{-1}, and (e) 1.0 wt.% of MWCNTs at 36.5 s^{-1}. The shear rates are the values on the wall.

These experimental results demonstrated that the addition of MWCNTs provides the strong orientation by a rapid crystallization even with 0.1 wt.% at 36.5 s^{-1}, although the orientation relaxation occurred immediately prior to the solidification for pure HDPE. Moreover, the pronounced orientation as *c*-structure (untwisted lamellae) was detected at this shear rate for the sample containing 1.0 wt.% of MWCNTs.

Besides the Weissenberg number for chain stretching, i.e., the product of strain rate and Rouse relaxation time, it has been well known that the applied work is a critical factor to form the shish-kebab structure.[12,17,40,41] Therefore, we used short and long dies for the capillary extrusion to confirm the contribution of the work in the capillary die. We characterized the structure in the extruded strands for pure HDPE and the blend containing 0.3 wt.% of

MWCNTs by 2D-WAXD. As shown in the supporting information, it was found that the length of the die hardly affects the oriented structure. This is reasonable because the MWCNTs behaved like extended chain crystals.

The orientation of both HDPE chains and MWCNTs seems to have been responsible for this marked oriented structure. Therefore, HDPE chains that are oriented to the flow direction can attach to the MWCNT surfaces without greatly altering their chain conformation; i.e., the actual surface area of the MWCNTs that is available for the attachment of HDPE chains increases when the orientation directions match. This situation enhances the epitaxy matching and thus suppresses the nucleation barrier as revealed by Patil et al.[23] The geometrical confinement, as demonstrated by Li et al.,[36] also contributes to enhance the crystallization in the flow field.

Owing to the increased molecular orientation of the HDPE, the MWCNTs produce a high tensile modulus in the flow direction. Fig. 10 shows the tensile storage modulus at 20 °C for the strands extruded at 36.5 s^{-1} as a function of the MWCNT content. It has been known that rigid fillers enhance the modulus even without changing the structure of a matrix polymer.[42] In this study, however, the moduli increased considerably with a significantly small amount of MWCNTs, suggesting that the chain orientation is mainly responsible for the modulus enhancement.

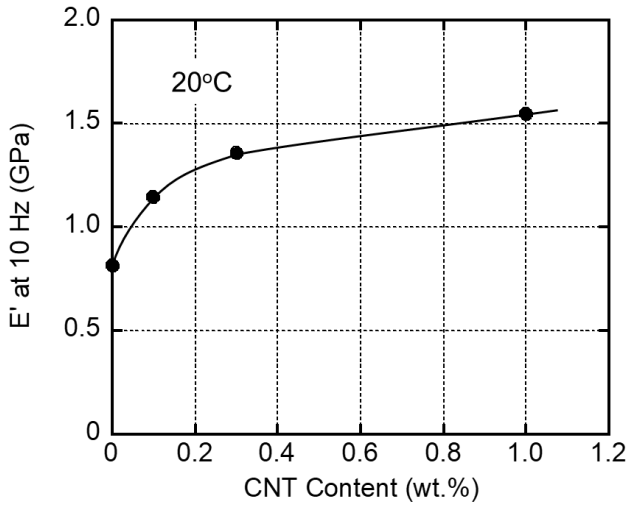

Fig. 10 Tensile storage modulus E' at 10Hz at 20 °C as a function of the MWCNT content for the strand extruded at 36.5 s^{-1} on the wall.

4. Conclusions

In the present study, we investigated the effect of MWCNTs on the structure of HDPE when it was extruded from a capillary rheometer. We found that the MWCNTs greatly increased the orientation of the PE chains with a slight increase in the crystallinity. The lamellae oriented perpendicular to the flow direction with twisting (0.1 and 0.3 wt.% of MWCNTs) or untwisting (1.0 wt.%). In contrast, there was no such orientation in HDPE without MWCNTs even at a high shear rate/stress condition. These results demonstrate that the orientation of the MWCNTs greatly affects the flow-induced crystallization of HDPE. One explanation for this is the matching of orientation between the HDPE chains and the MWCNTs. Furthermore, shish formation, which is the first step in flow-induced crystallization, is not required for HDPE containing MWCNTs, because the MWCNTs play a role on “shish”. They are also responsible for the rapid crystallization. The enhanced molecular orientation of the HDPE induced by the addition of MWCNTs increases the modulus in the flow direction greatly.

Acknowledgement

A part of this work was supported by JSPS Grant-in-Aid for Scientific Research (B) Grant Number 16H04201.

References

1. Iijama, S. *Nature* **1991**, *354*, 56.
2. Logakis, E.; Pandis, C.; Peoglos, V.; Pissis, P.; Stergiou, C.; Pionteck, J.; Pötschke, P.; Mičušík, M.; Omastova, M. *J. Polym. Sci. Part B Polym. Phys.* **2009**, *47*, 764.
3. Al-Saleh, M. H.; Sundararaj, U. *J. Polym. Sci. Part B Polym. Phys.* **2012**, *50*, 1356.
4. Ning, N.; Fu, S.; Zhang, W.; Chen, F.; Wang, K.; Deng, H.; Zhang, Q.; Fu, Q. *Prog. Polym. Sci.* **2012**, *37*, 1425.
5. Xiang, D.; Harkin-Jones, E.; Linton, D. *RSC Adv.* **2014**, *4*, 44130.
6. Liu, D.; Li, X.; Song, H.; Wang, P.; Chen, J.; Tian, Q.; Sun, L.; Chen, L.; Chen, B.; Gong, J.; Sun, G. *Eur. Polym. J.* **2018**, *99*, 18.
7. Keller, A.; Machin, M. J. *J. Macromol. Sci. Part B* **1967**, *1*, 41.
8. Odell, J. A.; Grubb, D. T.; Keller, A. *Polymer* **1978**, *19*, 617.
9. Schrauwen, B. A. G.; Breemen, L. C. A. V.; Spoelstra, A. B.; Govaert, L. E.; Peters, G. W. M.; Meijer, H. E. H. *Macromolecules* **2004**, *37*, 8618.
10. Choi, K.-J.; Spruiell, J. E.; White, J. L. *J. Polym. Sci. Part B Polym. Phys.* **1982**, *20*, 27.
11. Keum, J. K.; Zuo, F.; Hsiao, B. S. *Macromolecules* **2008**, *41*, 4766.
12. Mykhaylyk, O. O.; Chambon, P.; Impradice, C.; Fairclough, J. P. A.; Terrill, N. J.; Ryan, A. J. *Macromolecules* **2010**, *43*, 2389.
13. Yan, T.; Zhao, B.; Cong, Y.; Fang, Y.; Cheng, S.; Li, L.; Pan, G.; Wang, Z.; Li, X.; Bian, F. *Macromolecules* **2010**, *43*, 602.
14. Fernandez-Ballester, L.; Thurman, D. W.; Zhou, W.; Kornfield, J. A. *Macromolecules* **2012**, *45*, 6557.
15. Balzano, L.; Ma, Z.; Cavallo, D.; Van Erp, T. B.; Fernandez-Ballester, L.; Peters, G. W. M. *Macromolecules* **2016**, *49*, 3799.
16. Wingstrand, S. L.; Shen, B.; Kornfield, J. A.; Mortensen, K.; Parisi, D.; Vlassopoulos, D.; Hassager, O. *ACS Macro Lett.* **2017**, *6*, 1268.
17. Nazari, B.; Tran, H.; Beauregard, B.; Flynn-Hepford, M.; Harrell, D.; Milner, S. T.; Colby, R. H. *Macromolecules* **2018**, *51*, 4750.
18. Li, C. Y.; Li, L.; Cai, W.; Kodjie, S. L.; Tenneti, K. K. *Adv. Mater.* **2005**, *17*, 1198.
19. Patil, N.; Invigorito, C.; Gahleitner, M.; Rastogi, S. *Polymer* **2013**, *54*, 5883.

20. Chen, Y.; Wen, X.; Nie, M.; Wang, Q. *J. Vinyl Addit. Technol.* **2017**, *23*, 284.

21. Phulkerd, P.; Nakabayashi, T.; Iwasaki, S.; Yamaguchi, M. *J. Appl. Polym. Sci.* **2018**, *136*, 47295.

22. Liang, S.; Wang, K.; Chen, D.; Zhang, Q.; Du, R.; Fu, Q. *Polymer* **2008**, *49*, 4925.

23. Patil, N.; Balzano, L.; Portale, G.; Rastogi, S. *Macromolecules* **2010**, *43*, 6749.

24. Li, L.; Wang, W.; Laird, E. D.; Li, C. Y.; Defaux, M.; Ivanov, D. A. *Polymer* **2011**, *52*, 3633.

25. Wiwattananukul, R.; Hachiya, Y.; Endo, T.; Nobukawa, S.; Yamaguchi, M. *Compos. Part B* **2015**, *78*, 409.

26. Nishikawa, R.; Yoon, H.; Yamaguchi, M. *Nihon Reoroji Gakkaishi* **2019**, *47*, 150.

27. Yoon, H.; Okamoto, K.; Yamaguchi, M. *Carbon* **2009**, *47*, 2840.

28. Yoon, H.; Okamoto, K.; Umishita, K.; Yamaguchi, M. *Polym. Compos.* **2011**, *32*, 97.

29. Wiwattananukul, R.; Fan, B.; Yamaguchi, M. *Compos. Sci. Technol.* **2017**, *141*, 106.

30. Fan, B.; Wiwattananukul, R.; Yamaguchi, M. *Eur. Polym. J.* **2017**, *96*, 295.

31. Pötschke, P.; Fornes, T. D.; Paul, D. R. *Polymer* **2002**, *43*, 3247.

32. Pötschke, P.; Abdel-Goad, M.; Alig, I.; Dudkin, S.; Lellinger, D. *Polymer* **2004**, *45*, 8863.

33. Abdel-Goad, M.; Pötschke, P. *J. Non-newton. Fluid Mech.* **2005**, *128*, 2.

34. Macosko, C. W. *Rheology: Principles, Measurements, and Applications*; Wiley: New York, **1994**.

35. Yokohara, T.; Nobukawa, S.; Yamaguchi, M. *J. Rheol.* **2011**, *55*, 1205.

36. Li, L.; Li, C. Y.; Ni, C. *J. Am. Chem. Soc.* **2006**, *128*, 1692.

37. Seemork, J.; Itoh, T.; Nobukawa, S.; Yamaguchgi, M. *Nihon Reoroji Gakkaishi* **2016**, *44*, 23.

38. Seemork, J.; Sako, T.; Mohd Amran, B. M. A.; Yamaguchi, M. *J. Rheol.* **2017**, *61*, 1.

39. Fujii, Y.; Nishikawa, R.; Phulkerd, P.; Yamaguchi, M. *J. Rheol.* **2019**, *63*, 11.

40. Housmans, J.; Steenbakkers, R. J. A.; Roozemond, P. C.; Peters, G. W. M.; Meijer, H. E. H. *Macromolecules* **2009**, *42*, 5728.

41. Hamad, F. G.; Colby, R. H.; Milner, S. T. *Macromolecules* **2015**, *48*, 3725.

42. Nielsen, L. E.; Landel, R. F. *Mechanical Properties of Polymers and Composites, Second Edition*; CRC Press: Boca Raton, **1993**.